Effects of W^{6+} Doping of TiO_2 on the Reactivity of Supported Rh toward NO: Transient FTIR and Mass Spectroscopy Studies

Tarik Chafik,[†] Angelos M. Efstathiou,[‡] and Xenophon E. Verykios*

Department of Chemical Engineering, Institute of Chemical Engineering and High Temperature Processes, University of Patras, GR-26500 Patras, Greece

Received: May 9, 1997; In Final Form: July 26, 1997[⊗]

The transient adsorption and dissociation of NO over Rh supported on undoped and W^{6+}-doped TiO_2 in the temperature range of 25−450 °C has been studied by FTIR and mass spectroscopy. It was found that at 25 °C three kinds of adsorbed NO species are formed on the Rh surface of Rh/TiO_2 catalyst, namely $Rh-NO^+$ (1920 cm^{-1}), Rh−NO (1840 cm^{-1}), and $Rh-NO^-$ (1750 cm^{-1}), while several adsorbed nitrate species are formed on the TiO_2 support (1610−1240 cm^{-1}). On the other hand, in the case of Rh supported on W^{6+}-doped TiO_2, two additional infrared bands at 1680 and 1620 cm^{-1} are produced (not observed over W^{6+}-doped TiO_2 alone). The infrared band at 1680 cm^{-1} is suggested to be due to a $Rh-NO^-$ species adsorbed on a different site than that corresponding to 1750 cm^{-1}, while that at 1620 cm^{-1} is due to a nitrate species associated with an oxygen adatom on the Rh surface and a surface oxygen atom of the support. In the temperature range of 100−450 °C, the effect of carrier doping is to largely increase the extent of transient NO decomposition and selectivity towards N_2 formation. The influence of W^{6+}-doping of the TiO_2 carrier on the reactivity of Rh crystallites toward NO is discussed considering the fact that doping modifies the electronic structure of the TiO_2 carrier, which in turn modifies the electronic state of surface Rh atoms via electronic interactions at the metal−support interface. Furthermore, because of the significant enhancement of the concentration of oxygen vacancies in the W^{6+}-doped TiO_2, as compared to the undoped TiO_2 surface, oxygen adatoms formed by dissociation of NO on the Rh surface can migrate onto these vacancies at high temperatures. As a result, higher NO dissociation rates with prolonged reaction periods are obtained.

Introduction

The adsorption and reactivity of NO on supported rhodium catalysts have received particular attention by a large number of scientists because of the importance of NO reduction in the catalytic treatment of automotive exhaust gas streams.[1−3] Most of the information concerning the chemistry of the interaction of NO with Rh surfaces has been obtained by infrared spectroscopy. It has been established that NO adsorption on Rh surfaces gives rise to several nitrosyl-adsorbed species (infrared bands in the range of 1600−2000 cm^{-1}). Ari and Tominga[4] were among the first to study the chemisorption of NO on Rh surfaces. The infrared bands observed at 1910, 1810, and 1740 cm^{-1} were assigned to $RhNO^+$, RhNO, and $RhNO^-$ adsorbed species, respectively. Liang et al.[5] have classified three types of chemisorbed NO on Rh/Al_2O_3: The infrared bands at 1912 and 1648 cm^{-1} were assined to adsorbed $Rh-NO^{\delta+}$ and Rh−N═O (bent NO) species, respectively, while the infrared bands at 1825 and 1743 cm^{-1} were assigned to the symmetric and asymmetric stretching of dinitrosyl $Rh(NO)_2$ adsorbed species. The latter assignment is in contrast to that of neutral and negatively charged NO adsorbed species proposed earlier.[4] The $RhNO^+$ species has also been associated with the Rh^+ surface state.[4,6,7] The dissociation of adsorbed NO is considered by many researchers to be one of the key steps in the catalytic chemistry of the NO/CO reaction.[1,8−10] Pande and Bell[11] have found that over the Rh/TiO_2 catalyst NO chemisorption is suppressed with increasing catalyst reduction temperature, while NO decomposition to yield N_2O and N_2 increases with decreasing Rh dispersion.

The in situ characterization of the surface state of a catalyst by transient experiments, has proven to be a powerful tool which provides useful information concerning the nature and the role of the observed intermediate species in the reaction network.[12] The mass spectrometer, used as a detector, permits an accurate quantitative insight into the dynamics of the surface reaction processes. However, it is often difficult to know the exact nature of adsorbed intermediate species using only mass spectrometry. Transient FTIR spectroscopy is another powerful tool for studying the dynamics of surface reactions and identifying adsorbed intermediate species. Combining transient FTIR and mass spectroscopy offers the advantage of correctly characterizing surface reaction intermediate species (their chemical composition, surface coverage and reactivity).[13−16]

It is well-known that the chemisorptive and catalytic properties of supported metal catalysts can be altered by modifying the nature and composition of the support. For instance, doping of the support with altervalent cations can lead to such alterations. In particular, previous studies[17−20] have shown that the chemisorptive behavior of noble metal crystallites can be significantly altered by doping TiO_2 supports with altervalent cations. In addition, when Rh is supported on TiO_2 doped with small quantities of W^{6+} cations, enhanced catalytic activity for CO and CO_2 hydrogenation as well as for CO and C_2H_4 oxidation reactions has been observed.[18−21] The idea of doping a semiconductive carrier in order to enhance the catalytic activity of supported metal catalysts has recently been applied in the development of a more active "three-way" catalytic converter.[21,22] One of the components used is Rh dispersed on W^{6+}-doped TiO_2 carrier.

The focus of the present work is to investigate the influence of carrier doping on the adsorption and decomposition reactions of NO over Rh/TiO_2 and $Rh/TiO_2(W^{6+})$ catalysts. For this

* Corresponding author. Tel: +(3061) 991.527 Fax: +(3061) 993.255.
[†] Present address: Department of Chemistry, University of Tangier, P.O. Box 416, Tangier, Morocco.
[‡] Present address: Department of Natural Sciences, University of Cyprus, P.O. Box 537, Nicosia, Cyprus.
[⊗] Abstract published in *Advance ACS Abstracts,* September 15, 1997.

S1089-5647(97)01557-5 CCC: $14.00

purpose, various kinds of transient experiments, using mass and FTIR spectroscopies, have been conducted.

Experimental Section

Catalyst Preparation and Characterization. The parent titania carrier used in the present study was obtained from Degussa (P-25). X-ray diffraction analysis showed it to be 80% of the anatase form and 20% of the rutile form. To prepare the W^{6+}-doped TiO_2 carrier, weighed amounts of TiO_2 and WO_3 so as to yield 0.45 atom % W^{6+}, were slurried with distilled water and thoroughly mixed. The water was evaporated under continuous stirring and the residue was dried at 110 °C for 24 h. The dried material was then heated to 900 °C with a heating rate of 4 °C/min. It was maintained at 900 °C for 5 h and then slowly cooled to room temperature. During this heat treatment the doping cation (W^{6+}) diffuses into the crystal matrix of TiO_2, which is entirely transformed to the rutile form, as shown by XRD analysis. The 0.5 wt % Rh/TiO_2 and $Rh/TiO_2(W^{6+})$ catalysts were prepared by the method of incipient wetness impregnation using $RhCl_3 \cdot 3H_2O$ as the starting material. Details of the preparation procedure have been reported elsewhere.[18]

Metal dispersion of the Rh/TiO_2 catalyst was obtained by extrapolation of the linear part of the H_2 chemisorption isotherm at 25 °C to zero pressure, and was found to be 70% (34 μmol Rh_s/g_{cat}). Abnormal H_2 chemisorption behavior of Rh dispersed on TiO_2 doped with W^{6+} cations has been reported.[18] This behavior does not allow to estimate accurately Rh dispersion values over $Rh/TiO_2(W^{6+})$ catalysts from H_2 chemisorption results. On the other hand, TEM analyses performed over the undoped as well as the W^{6+}-doped catalysts revealed that the average Rh crystallite size of the doped catalyst was approximately 20% smaller than that of the undoped catalyst. Thus, Rh dispersion over the $Rh/TiO_2(W^{6+})$ catalyst is considered to be approximately the same as that of the Rh/TiO_2 catalyst.

FTIR Spectroscopy. The infrared spectrometer used in the present work is a Nicolet 740 FTIR equipped with a midrange TGS detector and a KBr beamsplitter. It was operated at a resolution of 4 cm^{-1}. Three to 32 interferograms were collected, depending on the time interval between successive scans. FTIR spectra recorded were baseline corrected and represented in Kubelka−Munk form. Spectra recorded with a clean catalyst surface under He flow at different temperatures were used as a background to which spectra recorded as a function of reaction temperature were corrected. In situ FTIR experiments were conducted in a Drift cell (Spectra Tech) which permits measurements to be performed in a controlled gas atmosphere and temperature. The infrared cell was equipped with ZnSe windows cooled by water circulating through blocks in thermal contact with them. A catalyst sample (50−70 mg) in finely powdered form was placed into a sample holder. The catalyst sample surface was carefully flattened in order to obtain high IR reflectivity. All gases (1% NO/He, Ar, and H_2) employed in the FTIR experiments were of ultrahigh purity. Hydrogen and Ar gases were further purified by passing them through oxygen traps which reduced the impurity level to less than 0.1 ppm.

Mass Spectrometry. Analysis of the gases during transient experiments was done by on-line mass spectrometer (Fisons, SXP Elite 300H) equipped with a fast response inlet capillary/leak diaphragm system. Calibration of the mass spectrometer was performed based on prepared gas mixtures of known composition. The output signal from the mass spectrometer was then converted to mole fraction, y (mol %). The integrity of the transient results, free of any flow disturbances caused by switching the chromatographic valves (use of electric actuators), was maintained as described elsehwere.[23] Nitric oxide (NO), nitrous oxide (N_2O), and dinitrogen (N_2) transients were recorded at $m/z = 30$, 44, and 28, respectively. The cracking coefficient of N_2O to the 28 peak (ratio of 28−44 peak) was determined based on 1% N_2O/He mixture passed in the mass spectrometer at the same source settings as those used at reaction conditions.

Reactor and Flow System for Transient Studies. The reactor used consists of two 4.0-mm-i.d. sections of quartz tubes which serve as inlet and outlet to and from a quartz cell of 7.0 mm i.d. (nominal volume 2 mL). The entrance to the reactor cell was machined in such a way as to create local gas mixing. Heating was provided by a small furnace controlled by a programmable temperature controller. The temperature of the catalyst sample is measured by a K-type thermocouple placed within a quartz capillary well in the middle of the catalyst bed.

An appropriate flow system that allows for the application of transient methods (abrupt switches in the feed gas composition) was employed in the present investigation. The main design features of this system have been described in detail elsewhere.[23] The NO/He gas mixture was of 1 mol % NO. The H_2 and He gases used were of ultrahigh purity (99.999%). Further purification of these gases was performed by using molecular sieve (13X) and MnO_x traps for removing traces of water and oxygen, respectively. The flow rate of all gases used was 30 mL/min (ambient).

Results

Interaction of NO with Rh/TiO_2 and $Rh/TiO_2(W^{6+})$ Catalysts Investigated by Transient FTIR. The transient characteristics of adsorbed species formed during NO interaction with the surface fo Rh/TiO_2 and $Rh/TiO_2(W^{6+})$ catalysts at 25 °C as a function of time on stream were studied as follows: The fresh catalyst sample was reduced in H_2 flow at 300 °C for 1 h and then purged in Ar flow at 300 °C for 30 min. The sample was then cooled in Ar flow to 25 °C. The feed was subsequently switched to 1% NO/He mixture. Figure 1a shows IR bands in the range of 1100−2100 cm^{-1} for times on stream of 1, 5, and 20 min. After 1 min on stream (spectrum A), two main IR bands at 1920 and 1750 cm^{-1} and two weak infrared bands at 1840 and 1610 cm^{-1} are observed. However, after 5 min on stream (spectrum B) several intense infrared bands below 1610 cm^{-1} appear (1585, 1540, 1490, 1293, and 1246 cm^{-1}), and an increase in the intensity of the IR bands at 1750 and 1920 cm^{-1} can be seen. By increasing the time on stream in NO/He from 5 to 20 min (spectrum C), the IR band at 1840 cm^{-1} disappears, and the IR bands at 1920 and 1585 cm^{-1} decrease, while those at 1490 and 1293 cm^{-1} increase.

The effects of doping of the TiO_2 carrier with W^{6+} cations on the chemical interaction of NO with Rh crystallites supported on it studied by FTIR are shown in Figure 1b. Immediately upon introduction of NO over the catalyst ($\Delta t = 1$ min, curve A) several IR bands are observed (1450, 1620, 1680, 1740, 1840, and 1920 cm^{-1}). By increasing the time on stream in NO/He, the IR band at 1840 cm^{-1} decreases, and after 10 min on stream it disappears completely. On the other hand, the IR bands at 1450, 1620, and 1740 cm^{-1} progressively increase with time on stream up to 20 min (curve D), while an IR band at 1320 cm^{-1} develops after 5 min on stream.

Figure 2a shows infrared spectra recorded during a temperature-programmed desorption (TPD) experiment (spectra B−E) following adsorption for 20 min (as described with respect to Figure 1a) and a 10-min treatment in Ar flow at 25 °C (Figure 2a, spectrum A) over the Rh/TiO_2 catalyst. During the latter gas treatment, no changes are observed in the infrared spectrum

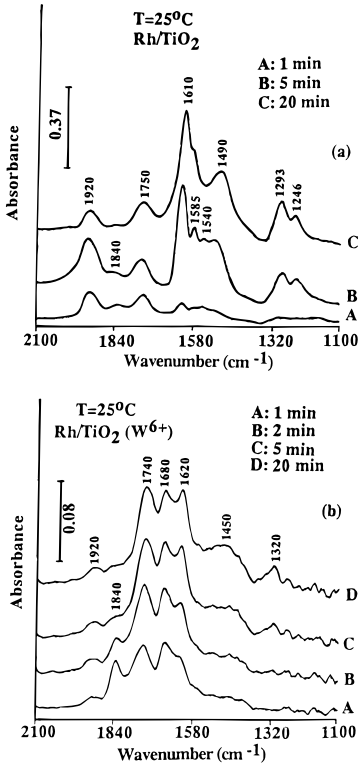

Figure 1. (a) Transient FTIR spectra in the range of 1100−2100 cm^{-1} recorded at 25 °C as a function of time on stream, Δt, in 1% NO/He over a reduced 0.5 wt % Rh/TiO_2 surface. Curve A, $\Delta t = 1$ min; curve B, $\Delta t = 5$ min; curve C, $\Delta t = 20$ min. (b) Transient FTIR spectra in the range of 1100−2100 cm^{-1} recorded at 25 °C as a function of time on stream, Δt, in 1% NO/He over a reduced 0.5 wt % $Rh/TiO_2(W^{6+})$ surface. Curve A, $\Delta t = 1$ min; curve B, $\Delta t = 2$ min; curve C, $\Delta t =$ min; curve D, $\Delta t = 20$ min.

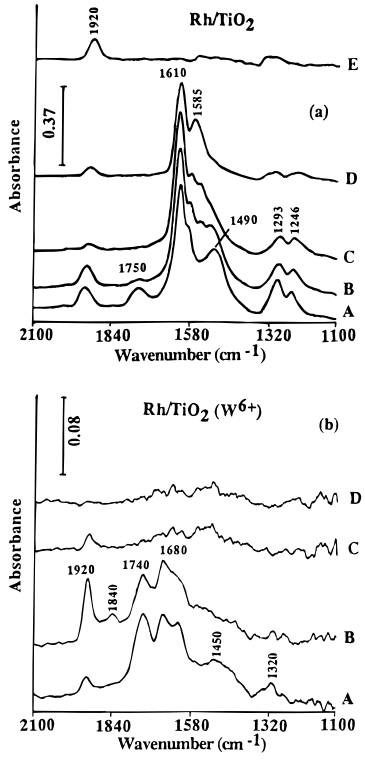

Figure 2. (a) FTIR spectra in the range of 1100−2100 cm^{-1} recorded during TPD in Ar flow following NO chemisorption at 25 °C for 20 min over Rh/TiO_2. Curve A, after 10 min Ar purge at 25 °C; curve B, after 5 min at 100 °C; curve C, after 5 min at 200 °C; curve D, after 5 min at 300 °C; curve E, after 5 min at 400 °C. (b) FTIR spectra in the range of 1100−2100 cm^{-1} recorded during TPD in Ar flow following NO chemisorption at 25 °C for 20 min over $Rh/TiO_2(W^{6+})$. Curve A, after 1 min Ar purge at 25 °C; curve B, after 5 min at 100 °C; curve C, after 5 min at 250 °C; curve D, after 5 min at 400 °C.

as compared to that obtained after 20 min of NO/He treatment at 25 °C (Figure 1a, spectrum C). On the other hand, by increasing temperature in Ar flow, large changes are observed. At 100 °C (spectrum B) the infrared band at 1750 cm^{-1} is drastically decreased, while the same behavior is observed at 200 °C (spectrum C) with respect to the IR band at 1920 cm^{-1}. As temperature in Ar flow increases from 200 to 400 °C the IR bands below 1620 cm^{-1} decrease, while the band at 1920 cm^{-1} starts to increase (compare spectra C−E). At the temperature of 400 °C (spectrum E) only the IR band at 1920 cm^{-1} is observed which is of approximately the same intensity as that observed at 100 °C (spectrum B). The FTIR spectra shown in Figures 1a and 2a probe for the transformation of NO from one adsorbed state to another with time of adsorption at 25 °C and also with temperature in Ar flow, up to 400 °C.

Figure 2b shows infrared spectra recorded during TPD following adsorption of NO at 25 °C for 20 min and 1-min Ar purge (curve A) over the $Rh/TiO_2(W^{6+})$ system. By increasing the temperature in Ar flow to 100 °C (curve B), the IR bands at 1320 and 1450 cm^{-1} disappear, and those at 1620, 1680, and 1740 cm^{-1} decrease, while the IR band at 1840 cm^{-1} starts to appear again. The latter feature is exactly opposite to the one observed during NO adsorption at 25 °C (development of IR band at 1840 cm^{-1} with time on stream). In addition, the IR band at 1920 cm^{-1} increases significantly at 100 °C, while, at higher temperatures, it starts to decrease and disappears at 400 °C (Figure 2b, spectrum D).

To further investigate these phenomena, similar experiments as those presented in Figure 1, a and b, were performed at higher temperatures. In the case of Rh/TiO_2 by increasing adsorption temperature to 250 °C (Figure 3a), the infrared bands at 1840 and 1750 cm^{-1} do not appear, as opposed to the case of adsorption at room temperature (compare Figures 1a and 3a). On the other hand, the intensity of the IR band at 1920 cm^{-1} is significantly higher than the corresponding ones observed at 25 and 100 °C after 20 min on stream. It was also observed that adsorption of NO at 450 °C produces only the IR band at 1920 cm^{-1} (spectrum not shown) which completely disappears after 10 min in Ar purge at 450 °C. Figure 3b presents the development of IR bands during NO/He exposure at 250 °C as a function of time on stream over $Rh/TiO_2(W^{6+})$. The nature of adsorbed species observed is the same as that obtained at 25 °C (Figure 1b). However, there are large differences in the relative proportion of the adsorbed species accumulated on the catalyst surface. In particular, after 1 min on stream the relative proportion of species corresponding to the IR band at 1920 cm^{-1} is significantly larger than that observed at 25 °C. It was also found that treatment of the catalyst with NO/He at 450 °C for 10 min produced only the infrared band at 1920 cm^{-1} whose intensity was found to be about twice that obtained with the Rh/TiO_2 catalyst. This result is consistent with the measurement of adsorbed NO species by mass spectrometry, to be described in a subsequent section. After 10 min in Ar flow at 450 °C, following adsorption at 450 °C, the infrared band at 1920 cm^{-1} was still observable.

The interaction of NO with TiO_2 and with W^{6+}-doped TiO_2, in the absence of Rh, was also investigated by FTIR spectroscopy. After 30 min treatment of the unmetallized TiO_2 surface with NO/He at 25 °C, five IR bands were observed (1246, 1293, 1540, 1585, and 1610 cm^{-1}; spectrum not shown), while the IR band at 1610 cm^{-1} appeared to be the most intense one. On the other hand, at higher adsorption temperatures (400 °C) only

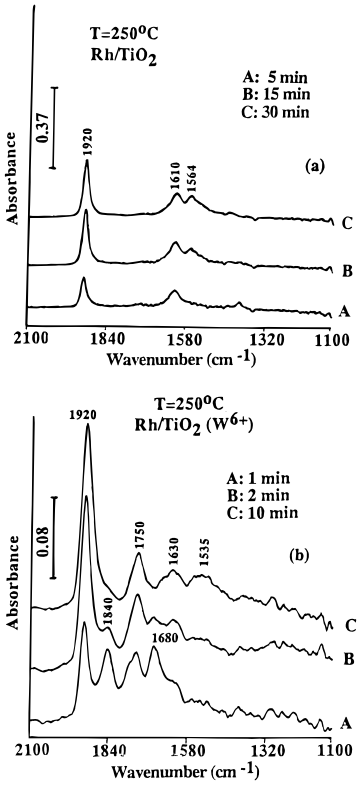

Figure 3. (a) Transient FTIR spectra in the range of 1100−2100 cm^{-1} recorded at 250 °C as a function of time on stream, Δt, in 1% NO/He over a reduced 0.5 wt % Rh/TiO_2 surface. Curve A, $\Delta t = 5$ min; curve B, $\Delta t = 15$ min; curve C, $\Delta t = 30$ min. (b) Transient FTIR spectra in the range of 1100−2100 cm^{-1} recorded at 250 °C as a function of time on stream, Δt, in 1% NO/He over a reduced 0.5 wt % $Rh/TiO_2(W^{6+})$ surface. Curve A, $\Delta t = 1$ min; curve B, $\Delta t = 2$ min; curve C, $\Delta t = 10$ min.

a small IR band at 1610 cm^{-1} was observed. Ar purge at 250 °C, following adsorption at 25 °C, was found sufficient to remove all the observed adsorbed species. Similar experiments performed with W^{6+}-doped TiO_2 revealed no detectable IR bands in the range of 1100−2100 cm^{-1}.

The transient FTIR results of the interaction of NO with the surface of Rh/TiO_2 and $Rh/TiO_2(W^{6+})$ catalysts revealed differences and similarities among the two catalytic systems with respect to the nature of the intermediate adsorbed species. Quantitative analysis of the interaction of NO with supported Rh crystallites is provided by similar transient adsorption and desorption experiments using a mass spectrometer as detector. The results obtained are presented below.

Transient Experiments with Mass Spectroscopy over Rh/TiO_2 and $Rh/TiO_2(W^{6+})$ Catalysts. The thermal stability and reactivity of adsorbed species, the latter accumulated during NO/He reaction at 25 °C, have been studied by temperature-programmed desorption (TPD) experiments, following the NO/He reaction. The amount of adsorbed nitrogen-containing species, the amount of gaseous reaction products formed, and the conversion and selectivity of NO decomposition under transient conditions over the 0.5 wt % Rh/TiO_2 and 0.5 wt % $Rh/TiO_2(W^{6+})$ catalysts have been determined by transient isothermal reaction experiments following the switch: He → NO/He(T, t), where t is the real time of the experiment. On-line mass spectrometry is used for the aforementioned experiments.

The thermal stability and reactivity of adsorbed nitrogen-containing species formed during 15 min of NO/He exposure at 25 °C was studied as follows: After the NO/He exposure, the feed was changed to pure He for 5 min and the temperature

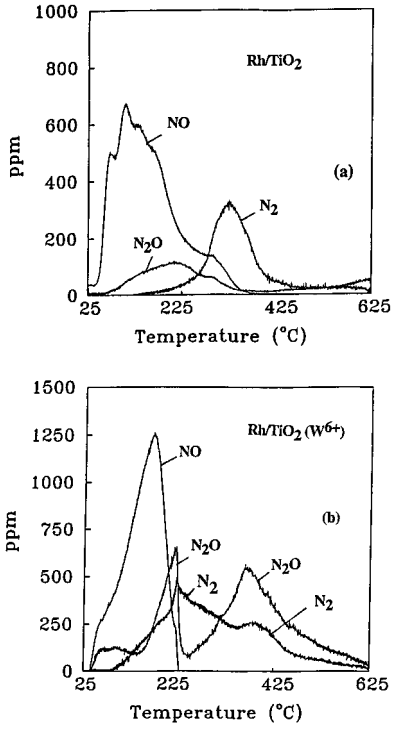

Figure 4. NO, N_2O, and N_2 responses obtained during a temperature-programmed desorption (TPD) experiment in He flow after 15 min of NO chemisorption at 25 °C followed by 3 min He purge at 25 °C. W = 0.5 g; $Q = 30$ mL/min (ambient); $\beta = 20$ °C/min. (a) Rh/TiO_2, (b) $Rh/TiO_2(W^{6+})$.

TABLE 1: Amounts (μmol/g_{cat}) of Species Formed during TPD following NO/He Reaction at 25 °C and 250 °C over 0.5 wt % Rh Supported on TiO_2 and W^{6+}-Doped TiO_2

	NO		N_2		N_2O		total	
T (°C)	A[a]	B[a]	A	B	A	B	A	B
25	12.1	14.6	5.2	12.6	3.6	16.6	20.9	43.8
250	2.0		1.3	3.2	1.2		4.5	3.2

[a] A: 0.5 wt % Rh/TiO_2. B: 0.5 wt % $Rh/TiO_2(W^{6+})$.

TABLE 2: Peak Desorption Temperatures following Adsorption of NO at 25 °C

catalyst	T_{NO} (°C)	T_{N_2O} (°C)	T_{N_2} (°C)
Rh/TiO_2	65, 100	205	320
$Rh/TiO_2(W^{6+})$	155	90, 210, 360	215, 380

of the catalyst was increased linearly ($\beta = 20$ °C/min) to 650 °C to carry out a TPD experiment in He flow. Figure 4a shows the NO, N_2O, and N_2 responses obtained during the latter experiment. The response of desorbed NO is rather complex showing two peak maxima at 65 and 100 °C and a shoulder at higher temperatures. A broad peak of N_2O is formed in the temperature range of 45−365 °C, while a second broad but smaller peak is obtained in the temperature range of 400−650 °C. On the other hand, a single symmetric peak of N_2 centered at 320 °C with a small tail-out to 625 °C is observed. The N_2O and N_2 responses shown in Figure 4a suggest that rather complex kinetics, involving several surface adsorbed intermediate species and reaction steps, lead to N_2O and N_2 formation. The amounts of gaseous species detected during TPD and the position of the peak maxima are summarized in Tables 1 and 2, respectively.

Figure 4b presents the NO, N_2, and N_2O responses obtained during TPD following 15 min of reaction in NO/He mixture at 25 °C (Figure 1b) over the $Rh/TiO_2(W^{6+})$ catalyst. All three gaseous responses exhibit large differences with respect to their

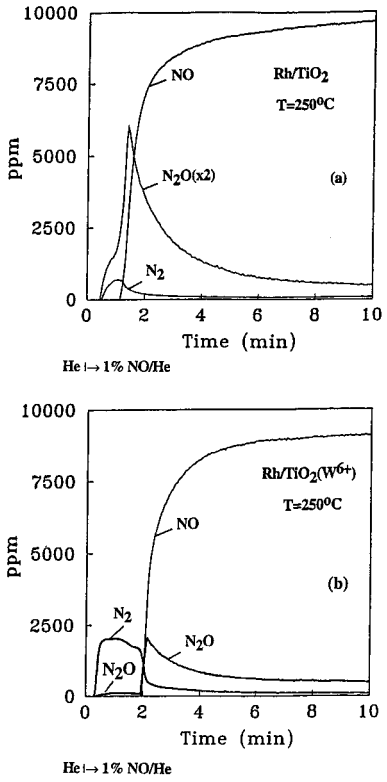

Figure 5. Transient responses of gas-phase NO, N_2O, and N_2 species obtained at 250 °C over (a) a reduced 0.5 wt % Rh/TiO_2 and (b) a reduced $Rh/TiO_2(W^{6+})$ surface. Gas delivery sequence: He → 1% NO/He(t). W = 0.5 g; Q = 30 mL/min (ambient).

shapes, position in the TPD spectrum, and amounts produced as compared to those obtained over the Rh/TiO_2 system (compare Figure 4, a and b, Table 1). Three distinct N_2O peaks are shown in Figure 4b, as compared to a rather broad N_2O TPD peak in Figure 4a. In addition, a larger amount of N_2 is produced during TPD at temperatures lower than 200 °C and also higher than 350 °C than in the case of the Rh/TiO_2 system. NO desorbs as a single peak (T_M = 155 °C) with a small shoulder at the rising part of it, and its desorption ceases at 225 °C. On the other hand, the NO response observed over the Rh/TiO_2 system consists of at least two peaks, while some NO desorbs in the range of 225−400 °C (see Figure 4a).

Figure 5a shows transient responses of gaseous NO, N_2, and N_2O after the switch He → 1% NO/He(t) is made at 250 °C over the reduced Rh/TiO_2 catalyst surface. The N_2 and N_2O product responses appear first, before the NO response, during the first minute of the transient. During this time, all of the NO fed in the reactor is consumed producing N_2 and N_2O as well as adsorbed nitrogen-containing intermediate species, while maxima in the production of N_2 and N_2O during the first minute of NO/He reaction appear (Figure 5a). As time on stream increases, gaseous NO appears at the outlet of the reactor, while the N_2 and N_2O yields drop significantly to smaller values. After 10 min on stream in NO/He, pseudo-steady state reaction rates are obtained (Figure 5a).

Based on an overall nitrogen material balance from t = 0 to t = 15 min, the quantity of adsorbed nitrogen-containing species (i.e., molecularly adsorbed NO according to the FTIR results of Figure 1a, and atomic nitrogen species) for the experiment presented in Figure 5a (15-min period) can be calculated and results are presented in Table 3, along with the overall conversion of NO and the overall selectivity toward N_2 formation of the reaction leading to gaseous products. The

TABLE 3: Amounts (μmol/g_{cat}) of NO Consumed and Nitrogen-Containing Species Adsorbed, as well as of N_2 and N_2O Gases Produced, after Reaction with 1% NO/He Mixture at Various Temperatures over 0.5 wt % Rh Supported on TiO_2 and W^{6+}-Doped TiO_2 Catalysts, Overall Conversion of NO into Gaseous Products, X_{NO}, and Overall N_2 Selectivity, S_{N_2}, for a Given Transient Reaction Period

T	$NO_{cons.}$		N-containing species		N_2		N_2O		S_{N_2} (%)		X_{NO} (%)	
(°C)	A[a]	B[a]	A	B	A	B	A	B	A	B	A	B
25	33.9	81.6	21.8	62.2			6.1	9.7	0.0	0.0	35.0[b]	22.0[b]
250	55.2	78.2	10.0	14.8	4.3	11.9	18.4	19.8	19[c]	37[c]	82.0[c]	81.0[c]
450	38.8	97.4	7.1	29.0	10.3	32.3	5.5	1.9	65[d]	94[d]	81.0[d]	65.0[d]

[a] A: 0.5 wt % Rh/TiO_2. B: 0.5 wt % $Rh/TiO_2(W^{6+})$. [b] During 15 min of reaction. [c] During 15 min of reaction. [d] During 10 min of reaction.

overall conversion of NO into gaseous products is given by eq 1,

$$X_{NO} = \frac{2\int_{t=0}^{t=15\ \mathrm{min}} (y_{N_2} + y_{N_2O})\,dt}{\int_{t=0}^{t=15\ \mathrm{min}} (y_{Ar} - y_{NO})\,dt} \times 100\ (\%) \qquad (1)$$

while the overall selectivity toward N_2 formation is given by eq 2.

$$S_{N_2} = \frac{\int_{t=0}^{t=15\ \mathrm{min}} y_{N_2}\,dt}{\int_{t=0}^{t=15\ \mathrm{min}} (y_{N_2} + y_{N_2O})\,dt} \times 100\ (\%) \qquad (2)$$

From the transient results shown in Figure 5a, an overall selectivity of the NO decomposition reaction to N_2, S_{N_2}, is estimated over a 15-min reaction time, following eq 2. This is found to be 19% and is reported in Table 3. The quantities (μmol/g) of NO consumed, adsorbed N-containing species, and N_2 and N_2O products formed over 15 min of the NO/He reaction at 250 °C are also reported in Table 3.

The effects of W^{6+} doping on the transient decomposition of NO at 250 °C are shown in Figure 5b. The N_2 and N_2O responses appear first upon introducing the NO/He mixture over the catalyst, while the NO response appears only after 100 s of reaction time. At this time, the N_2 response suddenly drops to a much lower value, while a sharp increase in the concentration of N_2O is observed. The drastic differences in the behavior of N_2O formation over the $Rh/TiO_2(W^{6+})$ and the Rh/TiO_2 catalysts (compare Figure 5, a and b), as well as the significantly larger S_{N_2} value (37 vs 19%) obtained over the former catalyst should be noted. There is also a larger amount of nitrogen-containing species accumulated on the $Rh/TiO_2(W^{6+})$ as compared to the Rh/TiO_2 surface (compare results shown in Table 3).

When the temperature of exposure of the catalyst to NO/He is increased to 450 °C, the transient responses of NO, N_2, and N_2O shown in Figure 6 are obtained. In the case of Rh/TiO_2 (Figure 6a), there is an overshoot in the production of N_2 and N_2O, whose concentrations are nearly constant for approximately 60 s of reaction time. During this period of time, no gaseous NO appears at the outlet of the reactor. After about 1 min of reaction, a sudden drop in the concentration of N_2 and N_2O appears which continues for about 10 min. At this time, the reaction almost ceases. The amounts of NO consumed, nitrogen-containing species accumulated on the surface, and N_2 and N_2O gaseous products formed over a 10-min transient period are reported in Table 3. Of importance is the much higher selectivity of the reaction to N_2 formation at 450 °C (S_{N_2} = 65%) as compared to the value obtained at 250 °C (S_{N_2} = 19%).

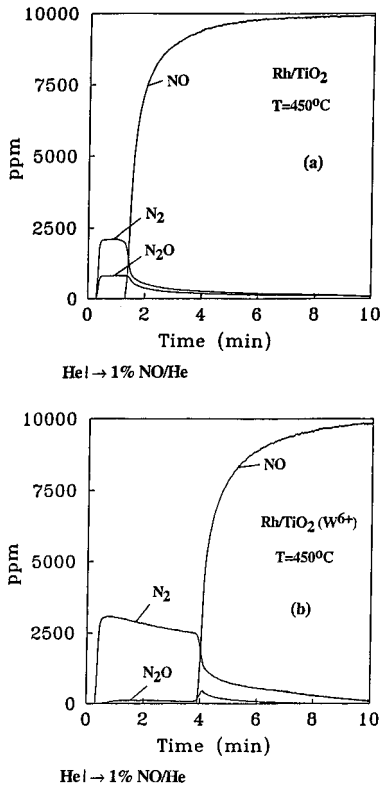

Figure 6. Transient responses of gas-phase NO, N_2O, and N_2 species obtained at 450 °C according to the gas delivery sequence: He → 1% NO/He(*t*) over (a) Rh/TiO_2 and (b) $Rh/TiO_2(W^{6+})$ catalyst surfaces. W = 0.5 g; Q = 30 mL/min (ambient).

Figure 6b shows the NO, N_2, and N_2O responses obtained after the switch He → 1% NO/He is made at 450 °C. As in the case of NO/He reaction at 250 °C, the N_2 and N_2O responses appear at the same time after the switch to NO/He is made. On the other hand, there is an approximate 200-s time delay in the appearance of NO at the outlet of the reactor, to be compared to a 60-s delay observed in the case of Rh/TiO_2 (compare Figure 6, a and b). In addition, over a period of 10 min of reaction, the amount of N_2 produced is about 3 times larger than that obtained over Rh/TiO_2, while the N_2O produced is only 35% of that obtained over the Rh/TiO_2 system. These results lead to a significant increase of S_{N_2} (94% vs 65%, Table 3).

Transient experiments similar to those reported in Figures 5 and 6 have been performed at 25 °C over both catalysts. At this temperature only a small amount of N_2O product was observed. The quantitative results of this experiment are reported in Table 3.

Discussion

The present work aimed toward obtaining a fundamental understanding concerning the enhanced catalytic activity of the NO/CO reaction over Rh when supported on W^{6+}-doped TiO_2 carrier.[21,22] The approach taken was to first study basic aspects related to the chemistry of interaction of NO itself with the surface of the doped and undoped catalysts, and then compare the information obtained with that of the NO/CO system. The transient results obtained with mass spectrometry (Figures 5 and 6) clearly indicate that the NO decomposition reaction leading to N_2 and N_2O gaseous products over both catalyst surfaces cannot be considered as true catalytic reaction. The surface state of the catalyst during the transient period is changing from that of a reduced one (H_2 reduction before reaction) to an oxidized one due to the inability of the system to remove the accumulated adsorbed surface oxygen species, produced by the dissociation step of adsorbed NO. However, these results, along with those obtained with FTIR spectroscopy, indicate that W^{6+} doping affects the kinetics of some important elementary steps encountered in the catalytic sequence of steps of NO reduction by CO.

TABLE 4: A Comparison of Adsorbed Species Formed over Rh/TiO_2, $Rh/TiO_2(W^{6+})$, and Rh/Al_2O_3 Catalysts after NO Chemisorption

type of NO species	infrared band (cm^{-1}) TiO_2[a]	Rh/TiO_2[a]	$Rh/TiO_2(W^{6+})$[a]	Rh/Al_2O_3	ref
$Rh-NO^+$		1920	1920	1910	4, 6, 7
$Rh-NO$		1840	1840	1830	4, 6, 7
				1825	1, 5, 24
				1743	
$Rh-NO^-$		1750	1740	1740	4, 6, 7
$Rh-NO^-$			1680	1660	4, 6
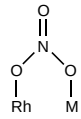			1620		
			1320		
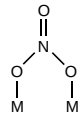	1610	1610			31−34
	1246	1246			M^b = Ti
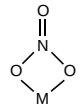	1585	1585			31−34
	1293	1293			M = Ti
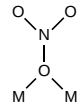	1540	1540		1550	4, 31−34
	1293	1293			
				1534	4, 16
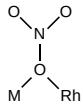		1490	1450		

[a] This work. [b] M: metal atom of support.

A. Effects of W^{6+} Doping on the Transient Nature of Adsorbed NO Species. The interaction of NO with the surface of Rh supported on undoped TiO_2 at room temperature produced three adsorption bands at 1920, 1840, and 1750 cm^{-1} (Figure 1a). These infrared bands are assigned to $Rh-NO^+$, $Rh-NO$, and $Rh-NO^-$ species, respectively, in agreement with earlier and recent attributions by many researchers, mainly from infrared studies on Rh/Al_2O_3.[4−8,16,24−26] Table 4 compares the infrared bands obtained in the present work (Rh/TiO_2 and $Rh/TiO_2(W^{6+})$) and those reported in the literature over the Rh/Al_2O_3 system upon NO chemisorption. The chemical structure corresponding to each assignment of infrared band is also shown. In addition, corresponding infrared bands and related chemical structures obtained over TiO_2 alone, in the present as well as in other investigations, are also reported in Table 4.

As time on stream in the NO/He mixture at 25 °C increases from 1 to 5 min, there is a significant increase in the intensity of the 1920 cm^{-1} IR band and, to a lesser extent, of the 1750 cm^{-1} IR band (Figure 1a). On the other hand, for longer times on stream (Δt = 20 min), there is a substantial decrease in the intensity of the 1920 cm^{-1} IR band, while the 1750 cm^{-1} IR

band remains practically constant. According to the literature,[24] the formation of $Rh-NO^+$ species (IR band at 1920 cm^{-1}) can arise from the adsorption of the NO molecule onto Rh−O sites according to the following reaction step:

$$Rh{-}O + NO(g) \longrightarrow Rh\begin{matrix}O\\ \diagdown\\ \diagup\\ NO\end{matrix} \qquad (3)$$

Upon introducing NO over the Rh/TiO_2 catalyst at room temperature, there is an accumulation of oxygen atoms on the Rh surface (by dissociation of NO), and, therefore, an increase in the concentration of Rh−O sites. Since adsorbed oxygen atoms cannot be removed from the Rh surface at 25 °C as dioxygen gas (not observed) or by other surface reactions (see reaction scheme in section B), it is expected that the surface coverage of atomic oxygen will reach a stable level after a given time on stream, and, consequently, the concentration of Rh−O sites. On the other hand, production of N_2O gas requires adsorbed NO species (see section B). It is, therefore, suggested that the decrease in the intensity of the IR band at 1920 cm^{-1} after 5 min on stream is due to the consumption of $RhNO^+$ species to form N_2O gas.

Solymosi et al.[6] have shown evidence that at room temperature NO can cause disruption of Rh_x clusters of the Rh/Al_2O_3 catalyst according to the following reaction:

$$Rh_x{-}NO \rightarrow Rh_{x-1} + Rh^+ + NO^- \qquad (4)$$

producing, therefore, oxidized Rh^+ sites. $RhNO^+$ can also be formed directly from NO adsorption on Rh^+ sites.[4,6,7] Thus, the occurrence of reaction 4 contributing to the development of the IR band at 1920 cm^{-1} cannot be excluded. However, Solymosi et al.[6] suggested that the formation of Rh^+ sites is accompanied by the formation of dinitrosyl species (IR bands at 1740 and 1830 cm^{-1}), since these bands were observed to gradually increase with time of exposure in NO. In the present case, however, the corresponding infrared band at 1840 cm^{-1} does not grow with increasing time on stream. It could then be argued that if the disruptive process of Rh_x clusters by NO does occur in the present case, the produced Rh^+ sites favor the formation of $RhNO^+$ and not of $Rh(NO)_2$ species. The infrared bands at 1840 and 1750 cm^{-1} are then mostly due to RhNO (neutral) and $RhNO^-$ species, respectively.[4−8]

In the case of $Rh/TiO_2(W^{6+})$, the adsorption of NO at 25 °C on the rhodium surface produces four infrared bands at 1920, 1840, 1740, and 1680 cm^{-1} (Figure 1b). As for the case of Rh/TiO_2 (Figure 1a), the infrared band at 1920 cm^{-1} corresponds to $RhNO^+$, that at 1840 cm^{-1} to RhNO (neutral), and that at 1740 cm^{-1} to $RhNO^-$. However, the IR band at 1680 cm^{-1} is not observed over the Rh/TiO_2 catalyst. This infrared band is suggested to be due to a $RhNO^-$ species associated with a site different than that corresponding to the IR band at 1740 cm^{-1}, in agreement with recent results of Srinivas et al.[26] on Rh/SiO_2.

The effects of doping of TiO_2 with W^{6+} cations on the chemisorptive and catalytic properties of supported Rh crystallites have been discussed in detail in the framework of the metal−semiconductor boundary layer theory.[17−20,27] The results of the present study, related to chemisorption of NO on Rh dispersed on undoped or W^{6+}-doped TiO_2 (Figure 1, a and b) can be explained based on those considerations as follows: The work function of Rh (ca. 5 eV) is higher than that of reduced TiO_2 (4.6 eV). When TiO_2 is doped with cations of higher valence (W^{6+}) its work function is further reduced. As a result, charge is transferred at the metal−semiconductor interface where the presence of short- and long-range interactions can perturb the electronic structure of the Rh crystallites.[27] The quantity of charge transferred depends on the concentration of the W^{6+} dopant in the TiO_2 carrier, and also on the gaseous environment under which the catalyst exists.[27] Thus, a rise in the Fermi level and a reduction of the chemical potential of the metal can take place which could be significant for small (1−5 nm) metal crystallites.[27] Enhancement of the electron density and reduction of the work function of the surface Rh atoms of the present Rh/TiO_2 (W^{6+}) system, is, therefore, expected to enhance the population of the 5σ orbital of the NO molecule and to increase the back-donation from the Rh d-orbitals to the 2π orbitals of NO, thereby strengthening the Rh−N bond and weakening the N−O bond. This mechanism is then in harmony with the appearance of the 1680 cm^{-1} infrared band in the case of $Rh/TiO_2(W^{6+})$ catalyst. Doping has apparently created new Rh sites with respect to their d-electron character, as compared to the Rh/TiO_2 case. These sites are most probably located at the interface of the Rh crystallites and the doped-TiO_2 carrier. However, considering the small size of the present Rh crystallites (<2.0 nm) it is likely that the electron structure of a large fraction of the surface Rh atoms is influenced by the doping process. Evidence for this can be obtained from the large intensity of the 1680 cm^{-1} IR band observed in Figure 1b.

It has also been pointed out[27] that the atoms at the periphery of the metal particles possess a high concentration of negative charge, while, in the same region, strong electrostatic fields are present due to the existence of a strong dipole at the metal−carrier interface. Such electric fields have been reported to influence the adsorption of NO on Rh(111) and Pt(111) surfaces in that a lower NO binding energy is obtained.[28−30] This effect would influence the relative population of the two $RhNO^-$ species observed on the rhodium surface supported on W^{6+}-doped TiO_2.

The differences in the relative population of the three kinds of NO species adsorbed onto the Rh crystallites supported on undoped and W^{6+}-doped TiO_2 are very important. The infrared results at room temperature (Figure 1), at which the dissociation of NO proceeds only to a small extent, strongly indicate that doping of TiO_2 with W^{6+} cations resulted in the creation of surface Rh sites with bonding orbitals of different d-character, as discussed previously. At higher adsorption temperatures, as the transient results of Figures 5 and 6 indicate, dissociation of NO is enhanced, and, since the oxygen atoms do not react on the Rh surface to give dioxygen gas, it is expected that the oxygen surface coverage increases with reaction temperature. This is expected to increase the relative concentration of Rh−O species, and, according to reaction step (3), of $Rh-NO^+$ species, with respect to the other adsorbed NO species. This is exactly what has been obtained in the FTIR results of Rh/TiO_2 and $Rh/TiO_2(W^{6+})$ catalysts. It is interesting to note that the development of $Rh-NO^+$ species with time on stream seems to coincide with the large decrease of Rh−NO (neutral) species which are known to be formed on reduced rhodium sites.[4] In addition, the observed progressive disappearance of IR bands due to $RhNO^-$ species with increasing adsorption temperature is strongly related to the higher propensity of $RhNO^-$ species to dissociate, relative to the other forms.

It is important to point out that in the present $Rh/TiO_2(W^{6+})$ system the amount of W^{6+} cations used in doping of TiO_2 correspond to 0.45 atom %, while doping of the titania matrix did occur.[17,18] At this level of doping the surface concentration of W^{6+} cations is very low as determined by XPS[17] and the possibility of bulk WO_3 formation must be excluded. Therefore, use of the incipient wetness method to deposit Rh onto the W^{6+}-doped TiO_2 surface must lead to Rh crystallites deposited onto the titania surface. The absence of any NO chemisorption onto

the unmetallized W^{6+}-doped TiO_2 surface strongly suggests that NO chemisorption on the $Rh/TiO_2(W^{6+})$ system takes place on the Rh surface. The role of W^{6+} cations is, therefore, that described previously in detail.

Adsorption of NO at room temperature over the Rh/TiO_2 surface produces infrared bands at 1610, 1585, 1540, 1490, 1293, and 1246 cm^{-1} which grow with time of exposure (Figure 1a, curves A−C). All the aforementioned infrared bands except the one at 1490 cm^{-1}, have also been observed over unmetallized TiO_2. The IR bands at 1610−1620 cm^{-1} are assigned to bridged nitrate species, in agreement with the literature.[31−34] Table 4 illustrates the structure of the proposed nitrate species. The infrared bands at 1585, 1490, and 1450 cm^{-1} can also be associated with nitrate ions of different coordination states.[31−34] In particular, the band at 1585 cm^{-1} can be associated with the bidentate form of nitrate species.[34] According to the work of Dines et al.,[34] the infrared band at 1246 cm^{-1} can also be assigned to nitrate species formed by the interaction of the NO molecule with surface oxygen atoms of TiO_2 (see Table 4). The fact that the IR bands at 1293 and 1246 cm^{-1} are absent in the case of $Rh/TiO_2(W^{6+})$ is related to the larger BET surface area of TiO_2 (anatase) as compared to that of W^{6+}-doped TiO_2 (calcined at 900 °C). In the case of $Rh/TiO_2(W^{6+})$, infrared bands at 1620 (strong), 1450 (weak), and 1320 (weak) cm^{-1} were observed. However, these bands were absent in the case of NO adsorption on the surface of W^{6+}-doped TiO_2 carrier. Based on the observations that the 1320 and 1450 cm^{-1} bands are observed neither on the unmetallized carrier (TiO_2 (W^{6+})) nor on Rh of the Rh/TiO_2 sample, these bands may be tentatively assigned to a nitrate species coordinated with Ti^{4+} and Rh atoms (see Table 4).

B. Effects of W^{6+} Doping on the Transient Decomposition Reaction of NO. The observed differences in the transient gas phase responses of NO, N_2 and N_2O obtained at 250 and 450 °C, following the switch He → 1% NO/He (Figures 5 and 6), over Rh supported on TiO_2 and W^{6+}-doped TiO_2 carriers can qualitatively be discussed with respect to the following sequence of elementary steps, which are based on results either obtained in this work or which have been reported in the literature.[1,3,35]

$$NO(g) + (s) \underset{k_1}{\overset{k_1}{\rightleftharpoons}} NO(s) \quad (5)$$

$$NO(s) + (s) \xrightarrow{k_2} N(s) + O(s) \quad (6)$$

$$NO(s) + N(s) \xrightarrow{k_3} N_2 + O(s) + (s) \quad (7)$$

$$N(s) + N(s) \xrightarrow{k_4} N_2(g) + 2(S) \quad (8)$$

$$NO(s) + N(s) \underset{k_{-5}}{\overset{k_5}{\rightleftharpoons}} N_2\,O(g) + 2(S) \quad (9)$$

Here, (S) is a site on the Rh surface. Assuming that the rate-determining step is that of NO dissociation (eq 6), as suggested by many investigators in the case of Rh catalysts,[1,8,10,26] the higher initial yield of N_2 observed over the $Rh/TiO_2(W^{6+})$ as compared to the Rh/TiO_2 catalyst can be attributed to either the higher initial surface coverage of adsorbed NO, or to the larger value of the rate constant, k_2, associated with this step, or to both. FTIR results obtained after 20 min of reaction with 1% NO/He mixture at 450 °C, followed by Ar treatment at 450 °C, revealed that the Rh−NO^+ species (the only kind of adsorbed NO species existing, 1920 cm^{-1}) disappear very fast in Ar flow at 450 °C over the Rh/TiO_2 catalyst, while they persist even after 10 min of Ar purge in the case of Rh/TiO_2-(W^{6+}) catalyst. In addition, it was also shown that at 250 °C $Rh/TiO_2(W^{6+})$ is populated by significantly higher amounts of Rh−NO^- species (IR bands at 1740 and 1680 cm^{-1}) than Rh/TiO_2 catalyst. These results support the view that the surface coverage of adsorbed NO at 450 °C might be larger in the case of $Rh/TiO_2(W^{6+})$ than Rh/TiO_2 catalyst, given the fact that Rh dispersion is similar in both catalysts.

On the other hand, despite the fact that the Rh−NO^- species are less thermally stable than the Rh−NO^+ species (see Figure 2), their nitrogen−oxygen bond is weaker than that corresponding to the Rh−NO^+ species. Thus, it is expected that dissociation of NO associated with the Rh−NO^- species would proceed with a higher rate than that corresponding to the Rh−NO^+ species, as also suggested by others.[8,10,26,36] The fact that there is no observable adsorbed Rh−NO^- species at 450 °C does not of course imply that this species does not participate in a dissociation step (eq 6); Srinivas et al.[26] have pointed out that the dissociation of Rh−NO^- species and the subsequent reaction between Rh−O and NO leads to the formation of

(Rh−NO^+ species) as shown by eq 3. The abovementioned observations suggest that at 450 °C the rate constant associated with the dissociation step of adsorbed NO is larger in the case of $Rh/TiO_2(W^{6+})$ than Rh/TiO_2 catalyst.

The transient behavior of the formation of N_2O gas as a function of temperature presents important information. First, the overall production of N_2O gas over both catalysts passes through a maximum in the temperature range of 25−450 °C (see Table 3). Second, the yield of N_2O gas at the initial stage of the transient is higher in the case of Rh/TiO_2 than the $Rh/TiO_2(W^{6+})$ system in the range of 25−450 °C, while the overall N_2O yield (at the end of the transient) is lower for the Rh/TiO_2 in the range of 25−250 °C but higher at 450 °C. These results strongly suggest the dependence of the rate of N_2O formation during NO decomposition on the surface state of Rh. During the initial stage of the transient, there is a higher fraction of the surface in the reduced than in the oxidized form (at $t = 0$, before the switch to NO/He mixture, the Rh surface is considered to be fully reduced). It can be suggested that W^{6+} doping greatly enhances the rate of N_2 formation and suppresses the rate of N_2O formation over a reduced Rh surface. As temperature increases from 250 to 450 °C, it might also be suggested that W^{6+} doping has a positive influence on the rate of N_2O decomposition via the reversible elementary step shown by eq 9.

Another important feature observed in Figures 5 and 6 is the effect of W^{6+} dopant in prolonging the time period since the start of the reaction, during which the yield of N_2 formation stays practically constant. This time period is found to be 0.9 min and 3.4 min in the case of Rh/TiO_2 (Figure 6a) and $Rh/TiO_2(W^{6+})$ catalyst (Figure 6b), respectively, for NO decomposition at 450 °C. It is important to state at this point that no dioxygen is formed at the conditions of the experiments presented in Figures 5 and 6. According to the elementary steps described by eqs 5−9, all oxygen produced by the dissociation of NO (eq 6) must stay on the catalyst surface. This is also confirmed by the fact that at 450 °C only the IR band corresponding to the Rh−NO^+ species is formed (see eq 3).

The amount of oxygen accumulated on the catalyst surface after 10 min of reaction with NO/He at 450 °C can be estimated based on the measurement of N_2 produced, considering that 1 gmol of N_2 formed corresponds to 2 gatoms of O accumulated on the surface. Based on the results presented in Table 3, the

Rh dispersion of the present catalysts (34 μmol Rh_s/g_{cat}), and assuming that one oxygen atom is bound on one Rh atom, it is found that the amount of oxygen atoms accumulated during the 10-min period of reaction corresponds to surface coverages of $\theta_0 = 0.6$ and 1.9 in the case of Rh/TiO_2 (Figure 6a) and $Rh/TiO_2(W^{6+})$ (Figure 6b), respectively. What must now be explained is the high value of θ_0 obtained when Rh is supported on W^{6+}-doped TiO_2.

It has been established[18] that the following defect−site reaction occurs when TiO_2 is doped with W^{6+} cations:

$$WO_3 \rightleftharpoons WO_2^{2+} + V_0'' + {}^1/_2O_2(g) + 2e^- \qquad (10)$$

where V_0'' represents the creation of an anionic vacancy and e^- a quasi-free electron. In addition, the following reaction can also be considered:

$$O + V''_0 + 2e^- \rightarrow O_0 \qquad (11)$$

where O is an oxygen atom on the Rh surface and O_0 is an adsorbed oxygen atom onto a vacancy of W^{6+}-doped TiO_2 carrier. Based on eqs 10 and 11, it is suggested that in the case of $Rh/TiO_2(W^{6+})$ catalyst, surface diffusion of adsorbed oxygen atoms, the latter produced by the dissociation of NO onto the Rh surface, toward oxygen vacancies present on the W^{6+}-doped TiO_2 carrier, can justify the amount of oxygen stored on the catalyst surface ($\theta_0 = 1.9$). This process also explains the larger period of time on stream before the conversion of NO starts to decrease as previously mentioned. As shown in Figure 6, the reaction almost ceases after about 10 min on stream. This result can be explained based on the fact that the process of oxygen transfer from the Rh surface onto the W^{6+}-doped TiO_2 carrier has a limited extent. It seems that only oxygen vacancies in the vicinity of the interface between the Rh crystallites and the support are energetically accessible at 450 °C.

The above discussion explains well the increase in the amount of NO consumed by increasing the temperature of reaction from 250 to 450 °C in the case of $Rh/TiO_2(W^{6+})$ system and the drop in the amount of NO consumed in the case of Rh/TiO_2 system (see Table 3). The beneficial role of W^{6+} doping, in keeping the Rh surface in a more reduced state is, therefore, rather clear. At temperatures higher that 450 °C, oxygen vacancies in the bulk of W^{6+}-doped TiO_2 could also be considered as another storage sink, increasing the degree of reduction of Rh surface during NO/He reaction. It is also important to note that W^{6+} doping did not have any beneficial effect on the recombination of adsorbed oxygen atoms to form dioxygen gas during high temperature NO decomposition reaction.

Chuang et al.[16] in their recent mechanistic study of NO−CO reaction over Rh/SiO_2 catalyst have pointed out that (a) $Rh-NO^-$ species are the most likely species to dissociate to adsorbed N and O, (b) the removal of O species occurs via elementary step 12

$$CO(s) + O(s) \rightarrow CO_2(g) + 2(S) \qquad (12)$$

and (c) NO dissociation is the rate-determining step of CO_2 formation. These important conclusions are related to the present work which addresses the question of the role of W^{6+}-doping in the NO−CO reaction over the $Rh/TiO_2(W^{6+})$ catalyst. The present work reveals that W^{6+} doping of titania causes a significant increase in the population of $Rh-NO^-$ species (Figure 1) over a reduced Rh surface. As a result of this, the rate of NO dissociation is enhanced. In addition, the higher dissociation rate of NO over $Rh/TiO_2(W^{6+})$ as compared to Rh/TiO_2 during NO−CO reaction may also be due to the higher degree of reduction of the Rh surface because of the removal of adsorbed O species by means other than the reaction step given by eq 12, as discussed in detail earlier.

C. Temperature-Programmed Desorption (TPD) Experiments. In the case of $Rh/TiO_2(W^{6+})$ catalyst, the N_2 response during TPD arises from two different sources: The first one is the pool of nitrogen atoms which are formed via the dissociation step (eq 6) during adsorption of NO at room temperature. The second source is part of the pool of adsorbed NO species which do not leave the surface as undissociated NO molecules. These two pools of surface adsorbed species can form N_2 gas according to eqs 7 and 8.

The infrared TPD results shown in Figure 2b can be utilized to interpret the TPD spectra obtained with mass spectrometry. According to these results, as temperature in He flow increases from 25 to 100 °C, the IR band due to $Rh-NO^+$ (1920 cm^{-1}) increases, while those bands corresponding to $Rh-NO^-$ (1740, 1680 cm^{-1}) decrease. In other words, there is an interconversion in the type of adsorbed NO species. At 250 °C, only the $Rh-NO^+$ species are still present on the Rh surface (Figure 2b, curve C). Based on these results, the appearance of the first N_2 peak ($T_{M_1} = 215$ °C) is due to the reaction of $Rh-NO^-$ species (1740 cm^{-1}) with nitrogen atoms (eq 7), while the appearance of the second N_2 peak ($T_{M_2} = 380$ °C) is due to the reaction step given by eq 8. The formation of this high-temperature N_2 peak may also arise via eq 7, where now the adsorbed NO species involved are of the $Rh-NO^+$ form. This possibility is supported by the formation of N_2O (third peak) in the same temperature range, where adsorbed NO is required (see eq 9). In analogy to the interpretation of the two N_2 peaks, and according to the IR results of Figure 2b, the low-temperature N_2O peak ($T_{M_1} = 90$ °C) is associated with the $Rh-NO^-$ (1680 cm^{-1}), the second peak ($T_{M_2} = 210$ °C) with the $Rh-NO^-$ (1740 cm^{-1}), and the third peak ($T_{M_3} = 360$ °C) with the $Rh-NO^+$ (1920 cm^{-1}) species. The infrared TPD results of Figure 2b and those obtained under NO/He flow in the range of 250−450 °C have clearly indicated that over the present catalysts the $Rh-NO^+$ adsorbed species have the highest thermal stability among all adspecies formed. This may imply that the rhodium−nitrogen bond in the $Rh-NO^+$ structure is the strongest among the other structures of adsorbed NO.

Larger amounts of NO desorb in the low-temperature range of the TPD in the case of Rh/TiO_2 than in the case of $Rh/TiO_2(W^{6+})$ (see Table 1). Furthermore, significantly larger amounts of N_2O are formed at higher temperatures in the case of $Rh/TiO_2(W^{6+})$ than Rh/TiO_2. These TPD results are in harmony with the infrared TPD results shown in Figure 1 and with the fact that an Ar purge at 450 °C following adsorption at 450 °C removed the IR band at 1920 cm^{-1} from the Rh/TiO_2 but not from the $Rh/TiO_2(W^{6+})$ catalyst. It appears that the $RhNO^+$ species are thermally more stable on $Rh/TiO_2(W^{6+})$ than on Rh/TiO_2 catalyst. The reason may be the different oxidation state of Rh in the two catalysts which is affected by the oxygen coverage produced by the dissociation of NO, and also the strengthening of the Rh−N bond due to W^{6+} doping of the carrier, as discussed in detail previously.

A single N_2 peak at a similar position as the one shown in Figure 4a has also been observed by Pande and Bell[11] over a 4.3% Rh/TiO_2 catalyst, and also by Kaspar et al.[37] over a Rh/Al_2O_3 catalyst. The high-temperature long tailing of the N_2O peak was also observed in other studies.[11,37] It is suspected that this may be due to the reverse reaction of NO dissociation (eq 6) followed by the reaction step given in eq 9.

Pande and Bell[11] have studied the effects of reduction temperature and metal dispersion of a Rh/TiO_2 catalyst on the NO interaction. They have found that the extent of NO decomposition increases with decreasing Rh dispersion. The effect of catalyst reduction temperature in H_2 flow was to drastically alter the kinetics of NO desorption and surface decomposition reactions leading to N_2 and N_2O products. They have attributed these alterations to the degree of decoration of the Rh surface by TiO_x species, the latter migrated from the support to the Rh surface during high-temperature reduction treatment. These TiO_x species were responsible for the creation of new sites for adsorption of NO. It is important to mention here that in the present study, the low-temperature hydrogen reduction applied ($T = 573$ K) is not sufficient to induce reduction of the surface of titania and surface decoration of Rh by TiO_x species.

Conclusions

The following conclusions may be drawn from the results of the present work concerning the interaction of NO with $Rh/TiO_2(W^{6+})$ catalyst surfaces:

1. Adsorption of NO at 25 °C over Th/TiO_2 produces three IR bands (1920, 1840, and 1750 cm^{-1}) associated with $RhNO^+$, RhNO, and $RhNO^-$ species, respectively. In the case of $Rh/TiO_2(W^{6+})$, in addition to these IR bands, a new strong IR band at 1680 cm^{-1} appears, associated with a second kind of $RhNO^-$ species. There is an interconversion among these species with adsorption time due to accumulation of atomic oxygen, formed by dissociation of adsorbed NO, which affects the oxidation state of Rh.

2. The $RhNO^+$ species are found to be the most thermally stable ones, compared to RhNO (neutral) and $RhNO^-$ species. W^{6+} doping of TiO_2 is found to enhance the thermal stability of $RhNO^+$ species on $Rh/TiO_2(W^{6+})$.

3. W^{6+} doping of TiO_2 promotes significantly the formation of $RhNO^-$ species (IR bands at 1680 and 1750 cm^{-1}) on the $Rh/TiO_2(W^{6+})$ surface. The N−O bond becomes weaker than that of the higher N−O stretching frequencies of adsorbed NO species (i.e., $RhNO^+$ (1920 cm^{-1}) and RhNO (1750 cm^{-1})). As a result of this, W^{6+} doping appears to promote the dissociation of adsorbed NO to N and O atoms.

4. In the temperature range of 250−450 °C, W^{6+} doping of TiO_2 is found to increase significantly the selectivity of the NO decomposition reaction toward N_2 formation, while, at the same time, the N_2O yield decreases significantly.

5. Adsorption of NO at 450 °C over both Rh/TiO_2 and $Rh/TiO_2(W^{6+})$ catalysts produces only $RhNO^+$ species (IR band at 1920 cm^{-1}) due to the high surface coverage of atomic oxygen species formed.

6. The yield of N_2 during the transient decomposition of NO at 450 °C is significantly increased in the case of $Rh/TiO_2(W^{6+})$ as compared to Rh/TiO_2 catalyst due to spillover of atomic oxygen species from the Rh surface to the oxygen vacant sites of the W^{6+}-doped TiO_2 carrier. This phenomenon controls the concentration of free Rh sites required for the dissociation of adsorbed NO and also the relative concentration of $RhNO^-$ to $RhNO^+$ species. The former NO species has a higher propensity to dissociate than the latter species.

References and Notes

(1) Shelef, M.; Graham, G. W. *Catal. Rev.—Sci. Eng.* **1994**, *36*(3), 433, and references therein.
(2) Armor, J. N. *Appl. Cata. B Environ.* **1992**, *1*, 221.
(3) Taylor, K. C. *Catal. Rev.—Sci. Eng.* **1993**, *35*(4), 457, and references therein.
(4) Ari, H.; Tominga, H. *J. Catal.* **1976**, *43*, 131.
(5) Liang, J.; Wang, H. P.; Spicer, L. D. *J. Phys. Chem.* **1985**, *89*, 5840.
(6) Solymosi, F.; Bansagi, T.; Novak, E. *J. Catal.* **1988**, *112*, 183.
(7) Dictor, R. *J. Catal.* **1988**, *109*, 89.
(8) Hecker, W. C.; Bell, A. T. *J. Catal.* **1983**, *84*, 200.
(9) Oh, S. H.; Fisher, G. B.; Carpenter, J. E.; Goodman, D. W. *J. Catal.* **1986**, *100*, 360.
(10) Krishnamurthy, R.; Chuang, S. S. C. *J. Phys. Chem.* **1995**, *99*, 16727.
(11) Pande, N. K.; Bell, A. T. *J. Catal.* **1986**, *97*, 137.
(12) Tamaru, K. *Dynamic Relaxation Methods in Heterogeneous Catalysis Science and Technology*; Anderson, J. R., Boudart, M., Springer Verlag: New York, 1991; Vol. 9 p 88.
(13) Efstathiou, A. M.; Chafik, T.; Bianchi, D.; Bennett, C. O. *J. Catal.* **1994**, *148*, 224.
(14) Efstathiou, A. M.; Chafik, T.; Bianchi, D.; Bennett, C. O. *J. Catal.* **1994**, *147*, 24.
(15) Yokomizo, G. H.; Bell, A. T. *J. Catal.* **1989**, *119*, 467.
(16) Balakos, M. W.; Chuang, S. S. C.; Srinivas, G. *J. Catal.* **1993**, *140*, 281.
(17) Akubuiro, E. C.; Verykios, X. E. *J. Catal.* **1987**, *103*, 320; **1988**, *113*, 106.
(18) Ioannides, T.; Verykios, X. E. *J. Catal.* **1994**, *145*, 479.
(19) Zhang, Z.; Kladi, A.; Verykios, X. E. *J. Phys. Chem.* **1994**, *98*, 6804.
(20) Zhang, Z.; Kladi, A.; Verykios, X. E. *J. Catal.* **1994**, *148*, 737.
(21) Papadakis, V. G.; Pliangos, C. A.; Yentekakis, I. V.; Verykios, X. E.; Vayenas, C. G. *Catal. Today* **1996**, *29*, 71.
(22) Vayenas, C. G.; Verykios, X. E.; Yentekakis, I. V.; Papadakis, V. G.; Pliangos, C. A. European Patent Appl. No. 94600002.3/28.01.94.
(23) Efstathiou, A. M.; Papageorgiou, D.; Verykios, X. E. *J. Catal.* **1993**, *141*, 612.
(24) Hyde, E. A.; Rudham, R.; Rochester, C. H. *J. Chem. Soc., Faraday Trans. 1* **1984**, *80*, 531.
(25) Solymosi, F.; Sarkany, *J. Appl. Surf. Sci.* **1979**, *3*, 68.
(26) Srinivas, G.; Chuang, S. S. C.; Debnath, S. *J. Catal.* **1994**, *148*, 748.
(27) Ioannides, T.; Verykios, X. E. *J. Catal.* **1996**, *161*, 560.
(28) Kreuzer, H. J.; Wang, L. C. *J. Chem. Phys.* **1990**, *93*, 6065.
(29) Block, J. H.; Kreuzer, H. J.; Wang, L. C. *Surf. Sci.* **1991**, *246*, 125.
(30) Madenach, R. P.; Abend, G.; Mousa, M. S.; Kreuzer, H. J.; Block, J. H. *Surf. Sci.* **1992**, *266*, 56.
(31) Hadjiivanov, K.; Bushev, V.; Kantcheva, M.; Klissurski, D. *Langmuir* **1994**, *10*, 464.
(32) Ramis, G.; Busca, G.; Lorenzelli, V.; Forzatti, P. *Appl. Catal.* **1990**, *64*, 243.
(33) Schramil, M.; Wokaum, A.; Baiker, A. *J. Catal.* **1992**, *138*, 306.
(34) Dines, T. J.; Rochester, C. H.; Ward, A. M. *J. Chem. Soc., Faraday Trans.* **1991**, *87*(4), 643.
(35) Belton, D. N.; DiMaggio, C. L.; Schmieg, S. J.; Simon Ng, K. Y. *J. Catal.* **1995**, *157*, 559, and references therein.
(36) Novak, E.; Solymosi, F. *J. Catal.* **1990**, *125*, 112.
(37) Kaspar, J.; de Leitenburg, C.; Fornasiero, P.; Trovarelli, A.; Graziani, M. *J. Catal.* **1994**, *146*, 136.